Thermodiffusion as a means to manipulate liquid film dynamics on chemically patterned surfaces

Sreeram K. Kalpathy[a) and Amrita Ravi Shreyes[b)
Department of Metallurgical and Materials Engineering, Indian Institute of Technology Madras, Chennai 600036, India

The model problem examined here is the stability of a thin liquid film consisting of two miscible components, resting on a chemically patterned solid substrate and heated from below. In addition to surface tension gradients, the temperature variations also induce gradients in the concentration of the film by virtue of thermodiffusion/Soret effects. We study the stability and dewetting behaviour due to the coupled interplay between thermal gradients, Soret effects, long-range van der Waals forces, and wettability gradient-driven flows. Linear stability analysis is first employed to predict growth rates and the critical Marangoni number for chemically homogeneous surfaces. Then, nonlinear simulations are performed to unravel the interfacial dynamics and possible locations of the film rupture on chemically patterned substrates. Results suggest that appropriate tuning of the Soret parameter and its direction, in conjunction with either heating or cooling, can help manipulate the location and time scales of the film rupture. The Soret effect can either potentially aid or oppose film instability depending on whether the thermal and solutal contributions to flow are cooperative or opposed to each other. *Published by AIP Publishing.* [http://dx.doi.org/10.1063/1.4984610]

I. INTRODUCTION

Dewetting of thin liquid films (~1–100 nm) on substrates with tailored heterogeneity has been recognized as a promising strategy for templating and nanopatterning.[1–5] When thin liquid films dewet physically or chemically patterned substrates, their dewetting mechanisms are more complex, as additional length scales pertaining to the pattern geometry need to be accommodated. This will also result in accelerated instability growth,[6–10] complex film morphologies, and/or different rupture locations, if any.[6,7,11–15] In many applications, the thin films of interest could consist of two miscible components, both of which have a specific role. A relevant emerging application is the creation of nanoscale functional structures based on polymer blends in photovoltaics and LEDs.[16–18] Another example is the mixing and separation of small quantities of two or more liquid components, relevant to micro- and nanofluidics,[19] and micro total analysis systems.[20] Especially important to these applications is an understanding of the flow dynamics and mass transfer when thin films of liquid mixtures dewet patterned surfaces.

Motivated by the above, we examine here a model problem where a thin liquid film mixture consisting of two miscible components is resting on a solid substrate, which may be chemically patterned by wettability differences (see Fig. 1). In addition, the film is subjected to vertical temperature gradients caused by heating or cooling the substrate, which induces flow by the thermal Marangoni effect.[21] This can not only accelerate the interfacial instability, but can even potentially

break the system symmetry.[22] As the film here consists of two miscible liquids, the applied temperature gradients will also drive the mass flux across the film, resulting in concentration gradients. This phenomenon, known as thermodiffusion or Soret effects,[23,24] may lead to a solutal flow contribution in a direction that could counteract the thermal Marangoni flow.[25] The dominant mechanism that governs the instability is then determined by the relative time scales of the two processes. Aside from these factors, it is well established that long range molecular forces, such as van der Waals attraction, lead to the rupture of ultrathin liquid films (≤100 nm) in finite time.[26,27] We also incorporate these long range forces in our model problem as the gradient of a potential (disjoining pressure) in the momentum balance equations, which is now accepted as a fairly standard approach. By varying the strength of the disjoining forces spatially along the width of the film, we model the practical situation where the bounding solid substrate is chemically patterned, based on the tendency of the liquid to wet/dewet the substrate.[9,28,29]

Recent experimental works[30–32] suggest methods by which significant temperature gradients can be sustained across ultrathin liquid films. For example, Dietzel and Troian[30] have demonstrated the formation of nanosized pillar arrays of poly(methyl methacrylate) by spin casting ~100 nm thick films of the polymer and heating the substrate, while simultaneously cooling the film from above. Similarly, polymer patterning on a sub-micron scale has been reported by Lyutakov *et al.*[33] using laser scanning in which the Marangoni effect introduced by light absorption is the proposed mechanism. In ultrathin liquid films on molten metals, Trice *et al.*[34] have shown experimental evidence via pulsed laser irradiation for thermocapillary-driven dewetting when film thicknesses are on the order of ~10 nm. These experiments also

---

[a)Author to whom correspondence should be addressed: sreeram@iitm.ac.in
[b)Current address: Department of Industrial and Systems Engineering, 3131 Texas A&M University, College Station, Texas 77843-3131, USA.
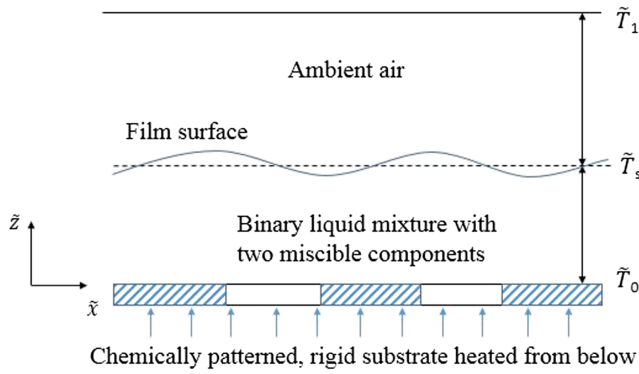
FIG. 1. Schematic representation of the problem setup. The hatched and unhatched areas represent alternating patches of more and less wettable regions on the solid substrate. Here $\tilde{T}_0$, $\tilde{T}_s$, and $\tilde{T}_1$ represent the temperatures of the solid substrate, film surface, and ambient air, respectively. The spatial variables are $\tilde{x}$ and $\tilde{z}$.

incite interest in theoretical models that examine combinations of thermal effects and long range molecular forces in thin films.[35–38]

We acknowledge here that problems involving stability analyses of thin films with miscible fluids have been attempted in the past.[39–46] However, these prior analyses have not examined the effects of induced temperature variations, which would cause Marangoni flows and Soret effects to significantly influence film dewetting. A host of long wavelength instability problems for binary liquid films including the interplay of Marangoni and Soret effects have been studied by Oron, Nepomnyashchy, and co-workers.[47–55] Two other notably important contributions which address these issues with the inclusion of gravity in the lubrication limit are the works by Bestehorn and Borcia[25] (linear stability analysis) and Borcia et al.[56] (fully nonlinear simulations). Our present work differs from these in two different ways. First, we generalize the results on linear stability analyses by adding an attractive van der Waals potential which these groups have not explicitly examined. Bestehorn and Borcia[25] have qualitatively mentioned that such potentials could help in promoting or preventing rupture when the film thickness is close to tens of nm, but not provided any detailed analysis. Second, we extend the nonlinear simulations of Borcia et al.[56] to explore the possibility of whether substrate chemical patterning could alter the dewetting behavior by confining liquid to certain areas. Other previous studies which examine the combined role of Marangoni and Soret effects pertain to thicker liquid films and for short-wave instabilities,[57,58] whereas our focus is on much thinner films where disjoining forces could be important.

II. PROBLEM FORMULATION

A. Problem geometry and assumptions

Figure 1 shows the schematic of the problem setup. A thin layer of a binary mixture comprising of two miscible liquids is bounded by a rigid solid substrate that is chemically patterned. The chemical patterning is such that the substrate has alternating patches which are more wettable or less wettable by the liquid above. The free surface of the liquid is exposed

to ambient air which is assumed to be a passive phase. The liquid mixture is assumed to be Newtonian and incompressible, and it has a uniform dynamic viscosity μ and density ρ. The substrate is heated (or cooled) from below such that its dimensional temperature is maintained constant, at a value $\tilde{T}_0$. The free surface of the liquid has a mean dimensional temperature $\tilde{T}_s$, and the ambient air much above the liquid surface has temperature $\tilde{T}_1$. In the case of heating the substrate from the bottom (or cooling the ambient air above), we would have $\tilde{T}_0 > \tilde{T}_s > \tilde{T}_1$, and in the case of cooling the substrate (or heating the air from above), we would have $\tilde{T}_1 > \tilde{T}_s > \tilde{T}_0$. The characteristic length scale in the horizontal direction (e.g., the wavelength of a typical interfacial perturbation) is denoted l (dimensional), which is assumed to be much larger than the characteristic vertical length scale d (dimensional), the mean film thickness. Thus we have the ratio $\epsilon = d/l \ll 1$, which allows us to employ the lubrication approximation. This implies that after scaling and non-dimensionalization, only leading order terms in ϵ will be retained in the governing equations (4)–(6) below.

The approach followed to derive the governing equations is very similar to the detailed derivation by Bestehorn and Borcia.[25] Here we show only some key equations and scalings to help the reader. We shall also highlight the key differences between their equations and ours, e.g., extra terms that arise due to the bottom surface being chemically patterned.

B. Scalings

The dimensional spatial coordinates $\tilde{x}$ and $\tilde{z}$ (see Fig. 1), and the dimensional time variable $\tilde{t}$ are scaled as follows:

$$\tilde{x} = lx, \qquad \tilde{z} = \epsilon l z, \qquad \tilde{t} = \tau t, \tag{1}$$

where $\tau = \rho l^2/\mu$ is the time scale of momentum diffusion. The dimensionless velocity components are $\tilde{u} = lu/\tau$ and $\tilde{w} = \epsilon l w/\tau$. As our focus in on a very thin film, we assume intermolecular forces like van der Waals forces to become important. They are introduced through the disjoining pressure potential $\tilde{V}$. The scalings for $\tilde{V}$ and the fluid pressure $\tilde{P}$ are chosen so as to reflect a balance between pressure gradients and viscous shear stress in the $\tilde{x}$-momentum balance equation,

$$\tilde{P}, \tilde{V} = \frac{\mu^2(P, V)}{(\epsilon^2 l^2 \rho)}. \tag{2}$$

The other variables pertaining to the liquid mixture are temperature $\tilde{T}$ and surface tension $\tilde{\Gamma}$. These variables are non-dimensionalized as

$$\tilde{T} = (\tilde{T}_0 - \tilde{T}_1)T, \quad \tilde{\Gamma} = \mu^2 \Gamma/(\epsilon \rho l). \tag{3}$$

The latter is chosen to scale capillary forces relative to viscous forces. The local relative concentration of one component of the mixture may be denoted as $\tilde{N}$, which is already a dimensionless quantity. Nevertheless we will use a rescaled version N, given by $\tilde{N} = \beta_N(\tilde{T}_0 - \tilde{T}_1)N$, where $\beta_N = -s_T \bar{N}(1-\bar{N})$. The quantity $s_T = D_T/D$ is the Soret coefficient which signifies the ratio of the thermodiffusion coefficient D_T to the mass diffusion coefficient D, and $\bar{N}$ is the mean relative concentration of the mixture.

C. Evolution equations

Using the scalings in Sec. II B, the dimensionless momentum balance equations along x and z in the lubrication limit are solved for the velocity components. The boundary conditions are no-slip at the solid surface, normal and tangential stress balances at the free surface, and the kinematic boundary condition at the free surface. When combined with the continuity equation, the evolution equation for the dimensionless film height $h(x, t)$ reads

$$-\frac{\partial h}{\partial t} = \frac{\partial}{\partial x}\left(\frac{h^3}{3}\bar{C}^{-1}\frac{\partial^3 h}{\partial x^3} + \frac{h^2}{2}\frac{\partial \Gamma}{\partial x} - \frac{A}{h}\frac{\partial h}{\partial x} + \frac{1}{3}\frac{\partial A}{\partial x}\right), \quad (4)$$

where $\bar{C}^{-1}$ is the inverse capillary number (see Table I), representing the importance of surface tension relative to viscous forces. Further, $A(x)$ is a parameter which represents the magnitude of van der Waals forces between the solid substrate and the free surface of the liquid. It comes into (4) through a disjoining pressure potential term $\sim A/h^3$ in the Navier-Stokes equation.[26,27] Negative values of A are chosen to represent attraction, while positive values would correspond to repulsion. The scaling for this parameter is $A = \tilde{A}\rho/(6\pi\mu^2\epsilon l)$. For a chemically homogeneous bottom surface, A would have the same connotation as the Hamaker constant.[59] In the present work, we set $A(x)$ to be a variable along the domain to model chemically patterned surfaces. This suggests that the magnitude of the van der Waals force can be different at different regions along the bottom surface, thus modulating the wettability.

The surface tension Γ in (4) is a function of both temperature and mixture concentration. Therefore, an appropriate energy equation and an equation for the concentration field N are needed in a lubrication form to complete the coupled system of equations. For temperature, the starting point is the heat transport equation accounting for convection and thermal diffusivity. The boundary conditions are the continuity of heat flux and temperature at the film surface. For concentration, the convection-diffusion equation is modified to include the thermodiffusion (Soret effect) and solved along with vanishing diffusive mass flux on the bottom ($z = 0$) as well as through the surface ($z = h$) as the boundary conditions. It turns out that the evolution equation for the concentration is conveniently expressed as the conservation of Φ, which is the cross-sectionally averaged concentration (i.e., integral of the zeroth order concentration $N^{(0)}$ over z),

$$\Phi(x, t) = \int_0^h (N - N_0)dz, \quad (5)$$

where N_0 is the value of N at $z = 0$ in the stationary, x-independent state (base state). The conservation equation for Φ reads

$$\frac{\partial \Phi}{\partial t} = \frac{\partial}{\partial x}\left[\frac{h^3}{3}\left(-\bar{C}^{-1}\frac{\partial^3 h}{\partial x^3} + \frac{3A}{h^4}\frac{\partial h}{\partial x} - \frac{1}{h^3}\frac{\partial A}{\partial x}\right)f - \frac{h^2}{2}\frac{\partial \Gamma}{\partial x}f \right.$$
$$+ Sc^{-1}h\frac{\partial f}{\partial x} + \frac{B}{1 + Bh}\left(\frac{5}{24}h^4\bar{C}^{-1}\frac{\partial^3 h}{\partial x^3} - \frac{5A}{8}\frac{\partial h}{\partial x}\right.$$
$$\left.\left. + \frac{5}{24}h\frac{\partial A}{\partial x} + \frac{h^3}{3}\frac{\partial \Gamma}{\partial x}\right)\right], \quad (6)$$

TABLE I. Description of various dimensionless parameters appearing in Eqs. (3)–(9). The range of values calculated here are obtained using properties of aqueous liquids or common polymeric solutions. Motivating values of common variables are $\epsilon \sim 10^{-3}$ to 10^{-2}, $l \sim 100\ \mu$m, viscosity μ in the range 10^{-3} to 1 mPa s^{-1}, and surface tension $\tilde{\Gamma} \sim O(10^{-2})$ Nm^{-1}.

Parameter	Symbol	Definition	Range of values used in the present work	Remarks
Marangoni number	M	$\frac{\epsilon\gamma_T(T_0-T_1)\rho l}{\mu^2}$	−1 to 10	For a 500 nm thick aqueous film, we would have $M \approx 3$, if $|T_0 - T_1| = 30$ K. Note that $T_o > T_1 \Rightarrow M > 0$ (heating from below), $T_o < T_1 \Rightarrow M < 0$ (cooling from below)
van der Waals parameter	A	$\frac{\tilde{A}\rho}{6\pi\mu^2\epsilon l}$	-10^{-2} to -10^{-5} and 10^{-5} to 10^{-2}	Attraction if $A < 0$, and repulsion if $A > 0$. Typical magnitudes of $\tilde{A}$ (dimensional) for real systems range between 10^{-18} to 10^{-21} J
Marangoni separation ratio	Ψ	$-\frac{\gamma_N}{\gamma_T}s_T\bar{N}(1-\bar{N})$	−1 to 1	Signifies ratio of surface-tension gradients due to thermodiffusion and thermal factors. See the discussion below Eq. (9) of Sec. II D
Schmidt number	Sc	$\frac{\mu}{\rho D}$	100	The ratio of momentum to mass diffusivity. For most realistic liquids, Sc would range from 10^2–10^4. The present analysis and Ref. 25 suggest that Sc in this range has little effect on instability growth rates
Biot number	B	$\frac{\epsilon l h_a}{\kappa}$	0.01	Here κ is the thermal conductivity of the liquid mixture and h_a is the heat transfer coefficient in air. The regime of practical interest is usually $B \ll 1$
Inverse capillary number	$\bar{C}^{-1}$	$\frac{\epsilon^3 l\bar{\Gamma}\rho}{\mu^2}$	10^{-6} to 10^{-5}	Here $\bar{\Gamma}$ is the mean value of surface tension, so that $\bar{C}^{-1}$ itself is a "constant." The practical regime of interest of $\bar{C}^{-1}$ lies between 10^{-7} to 10^{-2}

where B and Sc are the dimensionless Biot number and Schmidt number (see Table I). Setting Sc to infinity would imply that mass diffusion is absent. In our case, we retain mass diffusion by setting Sc to values much greater than unity, which conveys that momentum diffusion dominates mass diffusion. The function f in (6) has the definition

$$f(x, t) = \frac{\Phi}{h} + \frac{Bh}{2(1 + Bh)}. \tag{7}$$

D. Discussion

Equations (4) and (6) together represent a coupled system of two nonlinear evolution equations in h and Φ with x and t being the independent variables. In order, the various terms on the right hand side of (4) denote the relative contributions of capillarity, surface tension gradients, wettability, and wettability gradients.[9] Note that the second term $\partial\Gamma/\partial x$ would have both thermal and solutal (thermodiffusion) contributions. The evolution equations, (4) and (6), are same as the one-dimensional equivalents of Eqs. (48) and (49) in Ref. 25, with the exceptions that there is no gravity term here, and A is no longer a constant. The additional $\partial A/\partial x$ term is the key feature of our work, and it models patterned wettability. A smooth analytical arctangent function as used in prior works[9,28,29,60] is used to represent $A(x)$, which effectively delineates regions of the solid having larger and smaller values of A. This expression is described in Sec. IV.

A linear relationship is assumed to describe the variation of surface tension. In the dimensionless lubrication version at leading order, it may be expressed as[25]

$$\Gamma = \Gamma_0 + \frac{MB(1 + \Psi)h}{1 + Bh} - M\Psi f(x, t), \tag{8}$$

where Γ_0 is a constant and M is the dimensionless Marangoni number (see Table I), while $f(x, t)$ is defined by (7). Here Ψ is the Marangoni separation ratio, which physically signifies the ratio of solutal to thermal contribution in the deviation of surface tension from its mean value,

$$\Psi = -\frac{\gamma_N}{\gamma_T} s_T \bar{N}(1 - \bar{N}). \tag{9}$$

In general, γ_T would be negative, while the sign of γ_N and the Soret coefficient s_T would depend on the nature of thermodiffusion exhibited by the two liquid components. For example, s_T would be positive if the component measured by N migrates towards cooler regions and negative otherwise. In a realistic system like a water-isopropanol mixture in the ratio 10:1, we find that s_T is negative if N measures the relative contribution of water.[25] Together, the signs of γ_T, γ_N, and s_T would determine the sign of the separation ratio Ψ, which is a control parameter tunable between -1 and 1.

III. LINEAR STABILITY ANALYSIS

For chemically homogeneous surfaces (constant A), the initial growth characteristics of small amplitude surface perturbations are studied using a linear stability analysis. The base state for the height h and the cross-sectionally averaged concentration field Φ is chosen to be $h_0 = 1$ and $\Phi_0 = -\frac{B}{2(1+B)}$. The latter results from the assumption that both temperature and concentration profiles are linear in z. Setting $\frac{\partial A}{\partial x} \equiv 0$, the evolution equations, (4) and (6), are linearized with respect to $\hat{h}$ and $\hat{\Phi}$, the perturbations in h and Φ, respectively, around their corresponding base states. Upon using normal modes as

$$(\hat{h}, \hat{\Phi}) \sim \exp(ikx + st), \tag{10}$$

a quadratic equation for the perturbation growth rate s is obtained in terms of the wavenumber k,

$$s^2 + sk^2(a_3k^2 - a_1 - b_2) + a_2k^4(b_3k^2 - b_1) - b_2k^4(a_3k^2 - a_1) = 0. \tag{11}$$

The coefficients a_i, b_i ($i = 1, 2, 3$) are functions of the various dimensionless quantities and are given in the Appendix.

Inspection of (11) reveals that the growth rate s can in general be complex, and the system has both monotonic and oscillatory instability modes.[61] Figure 2(a) shows a phase map on the $M - \Psi$ space for heating from below ($M > 0$). For positive values of Ψ, we see that an oscillatory branch of instability comes first, as its boundary is at lower values of M. This oscillatory branch also extends continuously upwards as Ψ is decreased below 0, as shown in Fig. 2(b). However, we do note that for cooling from below ($M < 0$), only a monotonic instability exists. This is in a similar trend to the results for thicker films with gravity included, as observed by Bestehorn and Borcia,[25] although we do not encounter any Hopf bifurcation as they did.

Figure 3 shows a phase map on the $M - A$ space upon cooling the substrate from below ($M < 0$), for three different values of Ψ. As explained before, negative values of A
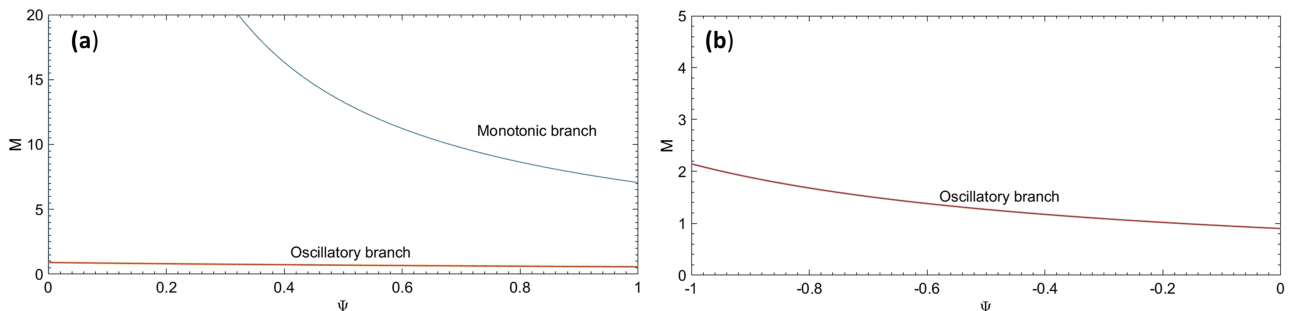

FIG. 2. (a) Stability map in the M-Ψ space for heating from below ($M > 0$). Other parameters are fixed at $A = -10^{-3}$, $B = 0.01$, $\bar{C}^{-1} = 10^{-5}$, and $Sc = 100$. The M-axis has been terminated at 20 deliberately for clarity in viewing the oscillatory branch. (b) The oscillatory branch in (a) extends continuously towards increasing M values when Ψ is decreased below 0. The monotonic branch is not shown.
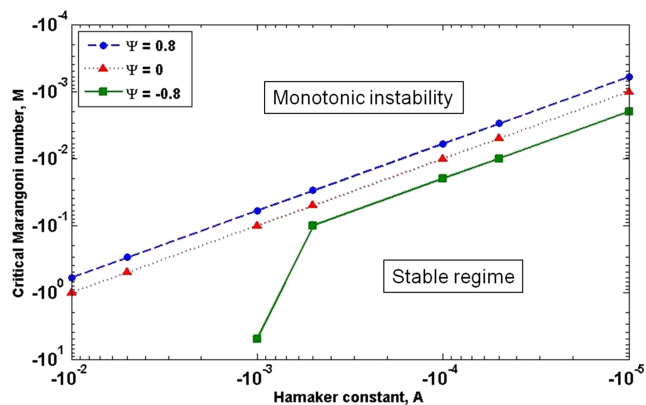
FIG. 3. Stability map in the M-A space for $\Psi = 0.8, 0, -0.8$. Other parameters are set to $B = 0.01$, $\bar{C}^{-1} = 10^{-5}$, and $Sc = 100$.

correspond to attractive van der Waals potentials. As Ψ decreases to more negative values, the critical value of M becomes more negative, indicating the film can be rendered stable in the presence of an attractive van der Waals force only upon adequately cooling the substrate relative to the film surface. As the separation ratio Ψ increases towards more positive values, the solutal contribution to flow acts cooperatively with the van der Waals force to promote the instability (see Sec. V B for details about different flow contributions). This results in an increase in the critical Marangoni number as Ψ is increased from -0.8 to $+0.8$, so that the film is stable even for slightly negative M. As mentioned earlier, the oscillatory branch is not seen here as it exists only for $M > 0$. Interestingly, for $\Psi = -0.8$ in Fig. 3, the film is always monotonically

unstable if the attractive van der Waals potential is stronger than a threshold ($A < -10^{-3}$). This is because the thermal and solutal contributions to flow are always opposed to each other when Ψ is negative. For large negative values of M, Marangoni flows prevent the instability while solutal contribution assists the van der Waals force.

Another interesting result based on linear stability analysis is that even for a stabilizing (repulsive) van der Waals potential (positive A values as in Table I), the critical Marangoni numbers for the onset of instability were found to be at most of O(1). These values are two orders of magnitude smaller in comparison to the results by Bestehorn and Borcia.[25] The departure might be explained using the inherent assumption that the initial film is thinner for disjoining forces to be more important in comparison to gravity, which in turn initiates instability even if the bottom substrate is heated slightly (and hence for lower values of M).

Figures 4 and 5 show the effect of intermolecular interactions on the growth rate maxima for three different values of Ψ: $-0.3, 0, 0.3$. Here we set $M = 0.5$, $B = 0.01$, $\bar{C}^{-1} = 10^{-5}$, and $Sc = 100$. In Fig. 4, an attractive van der Waals potential is considered ($A < 0$). The increased range of van der Waals attraction accelerates the growth rate as expected. The growth rates are also higher as the separation ratio is increased from negative values ($\Psi = -0.3$) towards positive values ($\Psi = 0.3$). This is suggestive of cooperative thermal and solutal flow contributions for positive values of Ψ and conflicting flow contributions for negative values of Ψ.

In Fig. 5, positive values have been deliberately chosen for A to model repulsive intermolecular forces (e.g., short range
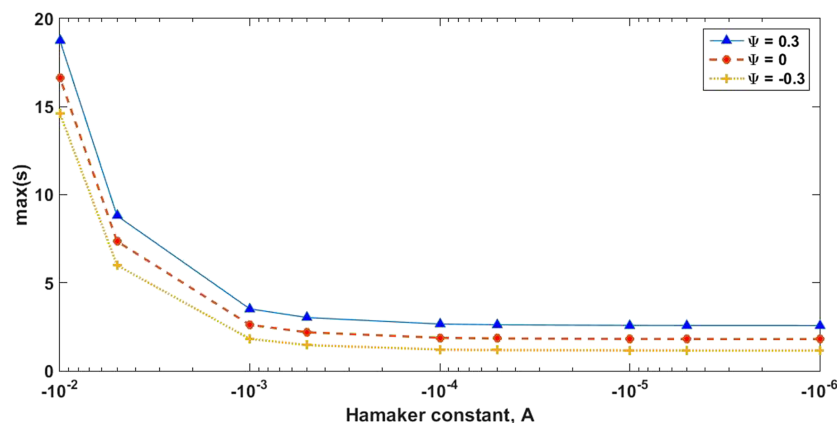

FIG. 4. The maximum in growth rate, as given by linear theory [Eq. (11)] for $M = 0.5$, $B = 0.01$, $\bar{C}^{-1} = 10^{-5}$, and $Sc = 100$, for negative (attractive) values of the parameter A.
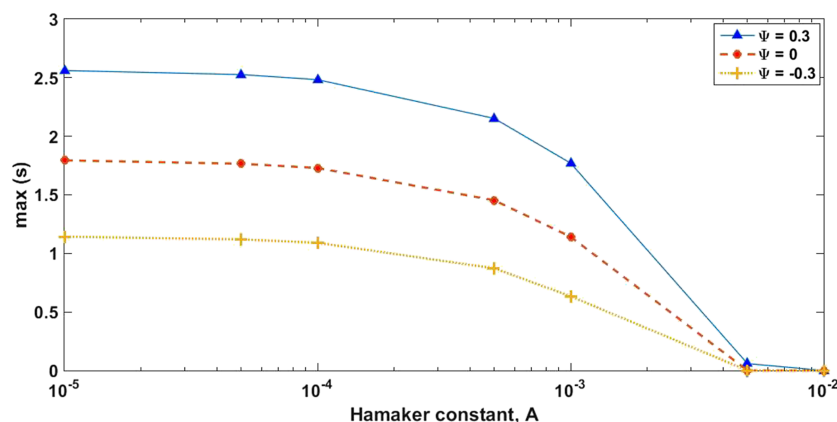

FIG. 5. The maximum in growth rate as given by linear theory [Eq. (11)] for $M = 0.5$, $B = 0.01$, $\bar{C}^{-1} = 10^{-5}$, and $Sc = 100$, for positive (repulsive) values of the parameter A.

electrostatic/steric interactions), though its exact mathematical form may not always be $\sim A/h^3$. In any case, such forces would drive liquid towards the depressions on the free surface of the film, whenever a rupture-like event is initiated by the thermal Marangoni instability. The growth of surface perturbations is then retarded, and more so when the magnitude of such repulsive forces increases (i.e., more positive values of A). The plots for all three values of Ψ approach $\max(s) = 0$ when the value of A is close to 10^{-2}. This indicates that the thermal Marangoni instability can be counteracted by sufficiently strong molecular repulsive forces for a given Marangoni separation ratio.

IV. NUMERICAL METHODS

The long-time evolution sequence of the film height and concentration for large amplitude surface perturbations was studied by the numerical integration of the evolution equations, (4) and (6). Time integration was performed using Differential Algebraic System Solver (DASSL), a package that employs backward differentiation formulae of orders one through five. The typical dimensionless time step used for the simulations was 10^{-7}. For the initial condition, the height h was perturbed using a single sine wave of dimensionless amplitude 0.1 about its base states $h_0 = 1$, while Φ was fixed at its base state $\Phi_0 = -\frac{B}{2(1+B)}$.

The wavelength used for the initial perturbation corresponds to that for which the growth rate s obtained from linear theory (Sec. III) is maximum. Hereafter, it is denoted as λ (dimensionless). It follows the same scaling for length as in Sec. II B. The length scales in our nonlinear simulations are mentioned in units of λ, which is assumed to be of $O(1)$. Therefore, the typical dimensional value for the wavelength will be approximately l, which we have chosen to be $\sim 100 \ \mu m$ (see Table I).

Whenever the rupture location was the specific question of interest, a random initial condition was employed. In this case, the initial perturbation was an average of Fourier modes with random phases and amplitudes, and a series of wavelengths ranging between $\lambda/100$ to 3λ. This was necessarily done while determining film profiles on chemically patterned surfaces.

Spatial discretization was achieved using a centered finite difference of fourth order accuracy with 1000 nodes per 3λ of the domain length. Periodic boundary conditions were employed for both the evolution equations, which would have a strong influence on film ruptures, as noted by Kargupta and Sharma.[13] Mass conservation was ensured by maintaining an average height of $h_0 \pm 0.001\%$ at all times during the course of the simulations. A minimum film height less than 5×10^{-2} was used as the criterion for rupture.

For modeling chemically patterned surfaces, the parameter A was varied along x using an analytical expression, adapted from prior work,[9,28,29,60]

$$A(x) = \frac{A_0}{\pi} \left[\tan^{-1}\left(\frac{x+w/2}{\delta}\right) - \tan^{-1}\left(\frac{x-w/2}{\delta}\right) \right]. \quad (12)$$

Figure 6 shows the variation of $A(x)$ as given by (12), plotted for $A_0 = -1$, $w = 0.5$, and $\delta = 0.01$ in the domain $-1 < x < 1$. The
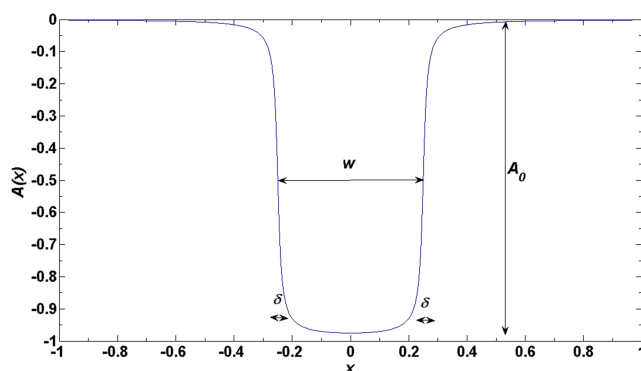

FIG. 6. Plot of (12) showing a typical variation of $A(x)$ by setting $A_0 = -1$, $w = 0.5$, and $\delta = 0.01$.

function closely resembles a step function with $A(x)$ approaching 0 at the left and right patches and approaching the value A_0 at a central patch of width w. The quantity δ is the transition width over which $A(x)$ changes the value from its minimum to its maximum. From a practical standpoint, the two-side patches on the left and right where $A \to 0$ would correspond to neutral zones which have no net attractive or repulsive potential. The central patch with $A \to -1$ would correspond to a region with an attractive potential between the film surface and the solid. For an aqueous film, the central patch on the solid would be a hydrophobic zone, as the attractive potential would cause the liquid to dewet this region. The value of A_0 may as well be set positive, in which case $A(x)$ would approach 0 at the left and right patches, and approach the corresponding positive value of A_0 at the center, denoting a repulsive potential. In that case, the central patch would represent a hydrophilic zone for an aqueous film. The steepness of the transition from $A(x) \to A_0$ to $A(x) \to 0$ may be increased by using lower values of δ. In the present work, we set $\delta = 0.01$ in all cases.

The validity of the long wave theory in the proximity of the wettability gradients is worth examining. For a mean initial film thickness of 100 nm and $\epsilon = 0.001$, our chosen value of $\delta = 0.01$ translates to a dimensional value of 1 μm for the transition width. This is still 10 times larger than the mean film thickness, and the patch widths w to be used in our simulations are even larger by at least an order of magnitude. Therefore, the long wave theory would still be expected to be valid to a large extent over the problem domain. Similar models have also been used in prior work,[9] and the justification therein for the validity of the model is also relevant in this context.

V. NONLINEAR DYNAMICS

It is important to emphasize that the highly nonlinear interactions between capillary forces, Marangoni forces, Soret effects, and van der Waals forces over long times of the film evolution can only be explicitly determined through nonlinear simulations. In particular, the linear theory cannot reveal the shape of the interface, which is especially important to know for dewetting on a chemically patterned substrate. Therefore we resort to fully nonlinear simulations, which will also reveal the likely rupture location, if any, and is also equally important

as the instability growth rates and rupture time. First, we briefly review the limit of a pure liquid film dewetting a patterned surface with and without Marangoni effects. We then compare this limit with the results for miscible liquids and distinguish between two situations: (i) heating the substrate relative to the film surface ($M > 0$) and (ii) cooling the substrate relative to the film surface ($M < 0$).

A. Rupture behavior of a pure liquid

For chemically patterned surfaces, the rupture and near-rupture locations are expected to be functions of the pattern width itself relative to the system's natural length scale λ.[6,9,12] In the case of a pure liquid film, one can broadly distinguish three different types of film profiles at rupture. Typically, if the pattern width w of the less wettable patch in the center was much smaller than λ, a single rupture event at the center is expected. This would be due to cooperation from the Marangoni flows, van der Waals forces, and wettability gradients. For an intermediate patch width, the wettability gradients

with assistance from Marangoni flows would try to cause near-rupture events at both the patch sides, but capillary forces oppose the formation of large curvatures at the center. This would result in two frustrated off-center ruptures (see Fig. 7 of Ref. 7 or Fig. 5 of Ref. 13). Note that the asymmetry about the center in the rupture profiles of Figs. 7, 9, 12, and 16 that follow, arises from the random initial conditions used.

For larger patch widths, independent ruptures are likely to occur at the ends of the patch, with some slight curvatures within them. When Marangoni forces are present, these curvatures would result in temperature variations at the film surface, causing additional flow outwards due to Marangoni effects. This difference is illustrated in Fig. 7, which shows film profiles at rupture when (a) Marangoni effects are absent ($M = 0$) and (b) Marangoni effects are present ($M = 1$). The profiles for a pure liquid film have been obtained by setting Φ to be constant and $f(x, t) = 0$ in (6) and solving it simultaneously with (4), with $M = 0$ for (a) and $M = 1$ for (b). In both cases, the pattern width w is set to 2.5λ out of the total domain
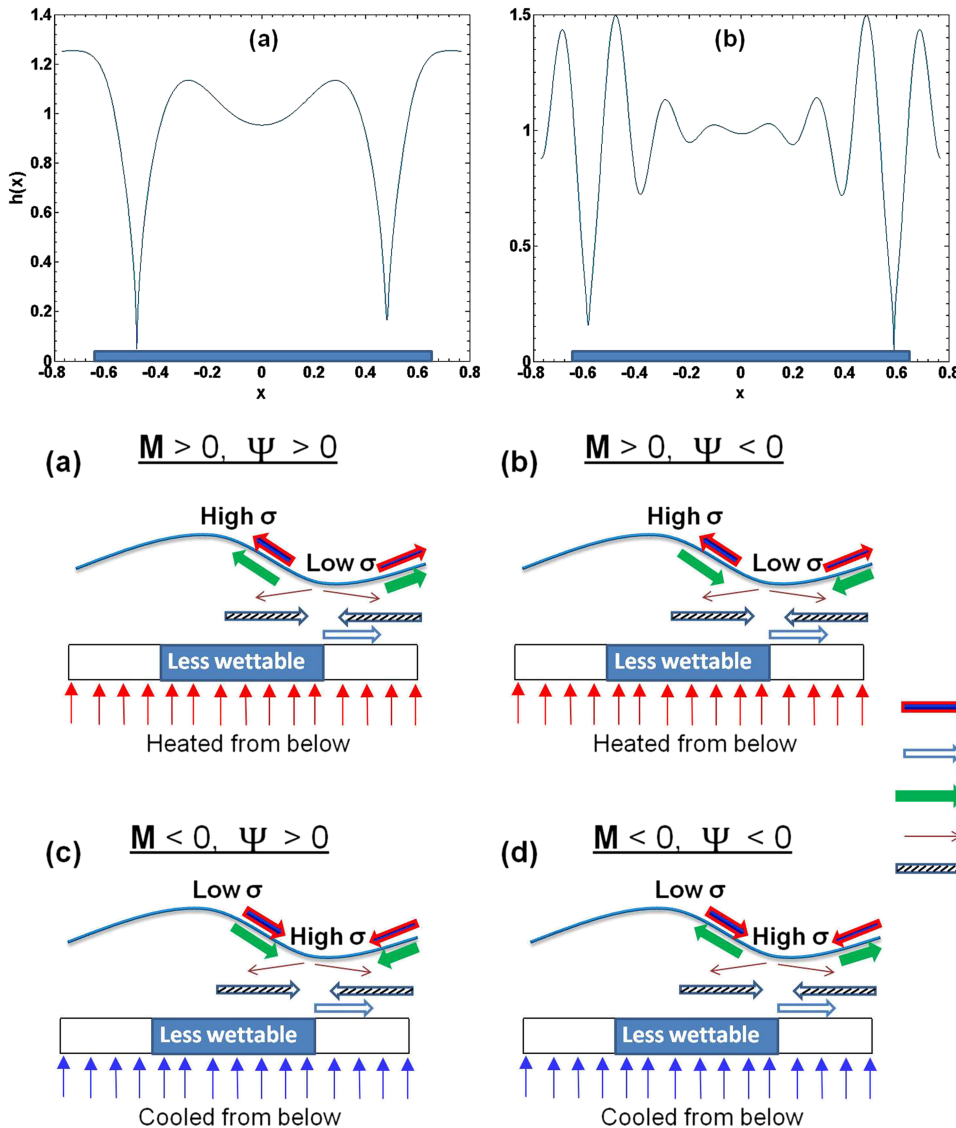

FIG. 7. Liquid film profile at rupture in the limit of a pure liquid, when (a) $M = 0$ and (b) $M = 1$. The domain length in each case is 3λ, and the central patch width of the less wettable zone (shaded region) is 2.5λ, where λ is the corresponding wavelength from linear theory. The other parameters used are $A_0 = -10^{-3}$, $\delta = 0.01$, $B = 0.01$, and $C^{-1} = 10^{-5}$.

FIG. 8. Schematic illustration of the directions of different flow contributions for the following cases: (a) $M > 0$, $\Psi > 0$, (b) $M > 0$, $\Psi < 0$, (c) $M < 0$, $\Psi > 0$, and (d) $M < 0$, $\Psi < 0$. The solid substrate is chemically patterned with a less wettable patch at the center. The curved line is the free surface of the liquid film.
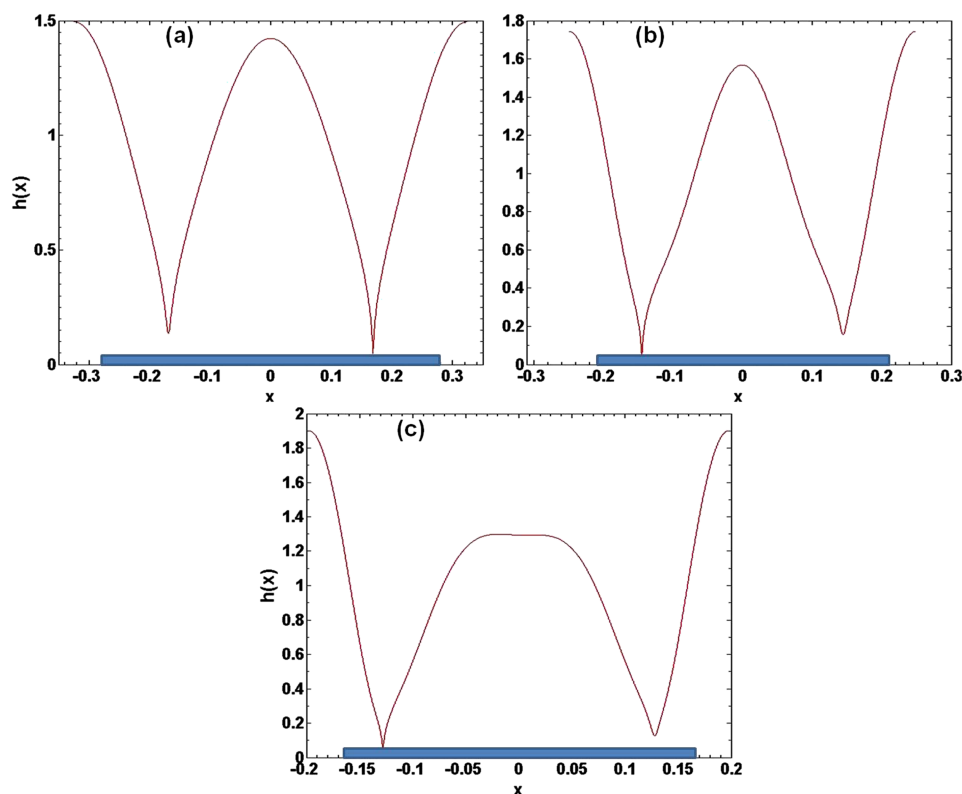
FIG. 9. Liquid film profile at rupture for a film of miscible liquids with $M = 1$, $Sc = 100$, and other parameters as in Fig. 7. The separation ratios are (a) $\Psi = -0.8$, (b) $\Psi = -0.2$, (c) $\Psi = +0.8$. The shaded region is the less wettable patch having width $w = 2.5\lambda$, while the total domain length is 3λ.

length 3λ. Further, we have used $A_0 = -10^{-3}$ and $C^{-1} = 10^{-5}$. Nearly simultaneous ruptures are seen at the ends of the pattern in each case, with the free surface being slightly curved (concave upward in both cases) as we approach the center of the domain. In Fig. 7(b), however, with $M = 1$, prominent depressions are seen on additional locations at the free surface due to extra thinning from Marangoni flows.[60] The configuration in the outer domain of Fig. 7(b) is different from that of the hump seen in Fig. 7(a) because now there is a driving force ($M = 1$) causing film thinning even in the outer region.

B. Parameter spaces for miscible liquids

If the heated film consisted of miscible liquids, the thermodiffusion effects could either aid or counteract the Marangoni flow contributions depending on the sign of the separation ratio Ψ.[25,56] For example, assuming γ_T in (9) to

be negative as in most liquids, a negative value of Ψ would result when $s_T < 0$ and $\gamma_N > 0$. By the convention used here (Sec. II D), $s_T < 0$ implies that the component measured by N migrates to warmer regions. This would counteract the thermal Marangoni flow, which would instead drive a flow from warmer regions (low surface tension) to cooler regions (high surface tension). Now, by heating or cooling the bottom substrate, the Marangoni flow itself can be used to either assist or counteract the patterned wettability gradients in causing the film rupture. Thus, one could in principle identify four interesting regimes of operation as follows: (i) $M > 0, \Psi > 0$, (ii) $M > 0, \Psi < 0$, (iii) $M < 0, \Psi > 0$, and (iv) $M < 0, \Psi < 0$.

Figure 8 schematically illustrates the directions of resulting flow contributions in each of the four parameter spaces. In (a) and (b), the bottom substrate is heated, and for a large enough pattern, near-rupture events would be initiated at the ends of the patch. The wettability contribution (attractive van der Waals forces) will cause the free surface to be pulled closer
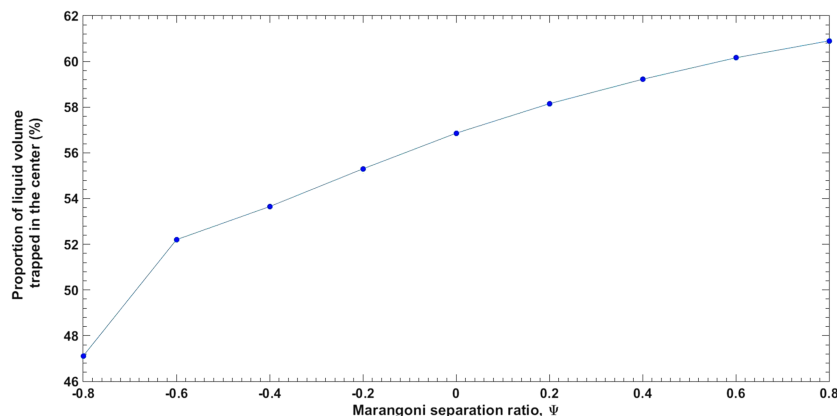

FIG. 10. Fraction of liquid volume trapped in the center at rupture, for a film of miscible liquids, as a function of the separation ratio Ψ. Other parameters used are as in Fig. 9.

to the substrate by removing liquid from both sides. This is accommodated by the upward Marangoni flow which drives liquid from warmer regions to cooler regions (pockets of lower surface tension to higher). In (a), the thermodiffusion contribution is in tune with the Marangoni flow, but in (b), both the effects counteract. When the bottom substrate is cooled relative to the film, as in (c), the downward Marangoni flow tends to replenish some of the liquid that is being removed by the wettability-driven flows. If Ψ is sufficiently positive, the solutal contribution would assist the thermal Marangoni contribution, whereas in (d), when Ψ is negative, both the effects again counteract.

C. Miscible liquids and *M* > 0

Figure 9 shows the rupture profiles for a film of miscible liquids, when thermal Marangoni effects ($M = 1$) and thermodiffusion ($\Psi = -0.8, -0.2, +0.8$) contributions are both present, with all other parameters the same as in Fig. 7. It may be remembered that this condition would be realized by either heating the substrate from below, or equivalently cooling the ambient air from above. In (a) and (b), the separation ratio is negative, so any near-rupture event assisted by the Marangoni flows would tend to be reversed by the solutal contribution [see Fig. 8(b)]. Any additional thinning within the central patch interiors would no longer be prominent. With more liquid trapped in the center, the free surface there at rupture assumes a concave downward shape with a large curvature. As Ψ changes to more positive values [Figs. 9(b) and 9(c)], the curvature decreases, and for $\Psi = 0.5$, a nearly flat interface results at the center. The fraction of liquid volume trapped in this case is higher when Ψ is more positive, as all three driving forces to rupture (van der Waals forces, Marangoni effects, thermodiffusion) are cooperative. This is evident from Fig. 10, which shows that the fraction of liquid volume trapped in the center increases from ~47% for $\Psi = -0.8$ to ~61% for $\Psi = +0.8$, for the same pattern width $w = 2.5\lambda$.

We next examine the time of rupture, which is an important parameter that could suggest variations in the rupture mechanism. Figure 11 shows the dimensionless rupture time for the parameters used in Fig. 9, as a function of the pattern width w for different separation ratios Ψ. Here w is the width of the less wettable patch in the center where rupture-like events are more likely to occur. It is given in units of λ, while the total
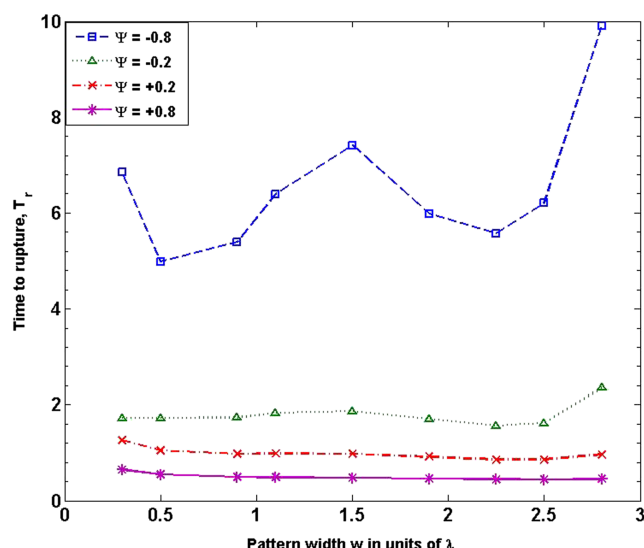

FIG. 11. Rupture time as a function of the pattern width w for different values of the separation ratio Ψ. Other parameters used are as in Fig. 9.

periodic domain length is 3λ. Rupture times are seen to be higher as Ψ becomes more negative, which may be attributed to the counteractive solutal flows that oppose any instabilities triggered by the thermal Marangoni effect. For $\Psi = -0.8$, the rupture time variation is similar to the manner seen in prior work with pure liquid films.[7,9] The local minima and maxima seen at specific pattern widths indicate regions where the driving forces (especially the van der Waals forces and capillarity) are either cooperative or conflicting, as discussed in Sec. V A.

As Ψ increases to more positive values, the variations in rupture time with w become minimal, as for $\Psi = +0.8$ where we note that the plot is nearly horizontal and flat. This is because for a pattern width $w = 2.5\lambda$, large curvatures are seen on the more wettable regions outside the central patch [Fig. 9(c)], just as large curvatures would be seen inside the central patch for smaller widths $w \sim 1.5\lambda$. In the latter case, frustrated off-center ruptures would result as seen in Fig. 7 of Ref. 7. In both these cases, there would be some resistance from capillary forces, which try to flatten out interfacial curvatures. On the contrary, for a pure liquid dewetting a pattern of width $w = 2.5\lambda$, the curvatures are not as large, both within the less wettable patch and the more wettable regions outside the central patch [see Fig. 7(a)]. Therefore, the capillary resistance experienced is
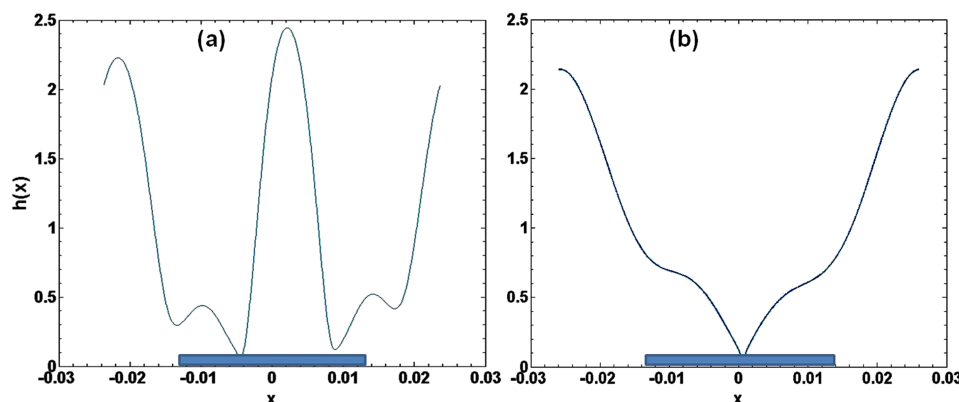

FIG. 12. Film height profiles at rupture for $M = 10$ and $w = 1.5\lambda$ (shaded region) for two different values of Ψ: (a) $\Psi = +0.5$ and (b) $\Psi = -0.5$, with other parameters same as in Figs. 9–11.
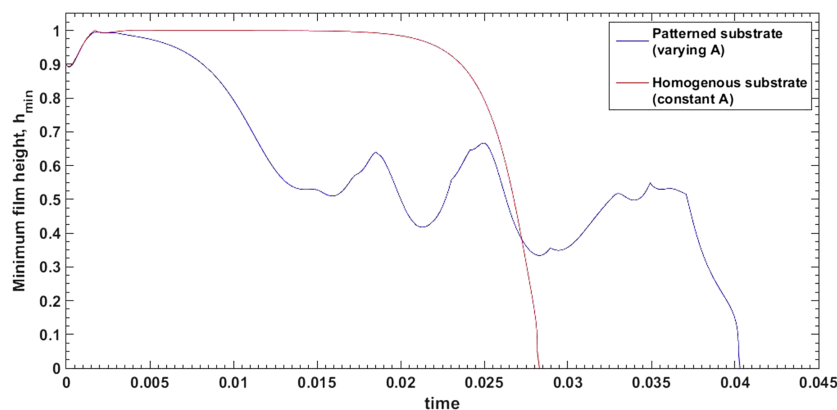
FIG. 13. The minimum film height as a function of time when $M = 10$ and $\Psi = -0.5$ for a homogeneous surface vs a chemically patterned surface having $w = 1.5\lambda$. Other parameters are the same as in Figs. 9–11. Note that minimum film heights at rupture are in the range 10^{-5}–10^{-6} but may appear to touch zero due to the y-axis scale used for the plot.

lesser, and the rupture is slightly faster for widths between 2λ and 2.5λ.

D. Other features of the instability

Figure 12 shows the film height profiles at rupture for $M = 10$ and $w = 1.5\lambda$ for two different values of Ψ: (a) $\Psi = +0.5$ and (b) $\Psi = -0.5$, with other parameters same as in Figs. 9–11. This pattern width is now smaller than that for which two independent ruptures can form, so two frustrated off-center ruptures would be expected for a pure liquid. This is also the result seen for miscible liquids with $\Psi = +0.5$ in Fig. 12(a). With Marangoni effects being stronger ($M = 10$), we also notice the emergence of secondary humps or "fingers" adjacent to the highly curved ridge at the center. This occurs when perturbations to the ridge cause mobility differences and results in uneven thinning of adjacent regions.[62]

In contrast, the rupture profile for the same pattern width in Fig. 12(b) ($\Psi = -0.5$) shows a single rupture near the center of the domain. Tracking the progressive time evolution sequence of the film in the latter case suggests that during the initial phases, localized holes and ridges that form are convected in arbitrary directions. At every time instance, a new fluid element at a different location corresponds to the minimum film height, until the minimum height is small enough for the van der Waals forces to dominate and cause rupture. This is the characteristic of an oscillatory instability. It occurs when the thermodiffusion effect is strong enough to induce large concentration gradients, and its nonlinear interplay with the patterned geometry is asymmetric about the center.

The minimum film height as a function of time for Fig. 12(b) ($\Psi = -0.5$) is plotted in Fig. 13, and the same is compared with the corresponding evolution on a chemically homogeneous surface. The non-monotonic variation seen for a chemically patterned substrate is consistent with the oscillatory behavior. The kinks in the curve for the patterned substrate represent the change in location and fluid element corresponding to the minimum film height. However, such an oscillatory behavior is found to result only within the selected $M - \Psi$ parameter space and selected pattern widths w. Consequently, the rupture can be delayed at these parameter values, by even a couple of orders of magnitude greater than the rupture time taken for a chemically homogeneous surface. A plot of the rupture time vs Ψ for a homogeneous and chemically patterned substrate ($w = 0.7\lambda$) is shown in Fig. 14. Wettability gradients on a chemically patterned substrate are known to be responsible for rupture times at least an order of magnitude smaller than those on homogeneous surfaces.[6–10] Therefore the present result suggests a possible mechanism by which these wettability gradients can be overcome to maintain a minimally thick film for longer times and also obtain newer templated structures for the same pattern size.

E. Miscible liquids and $M < 0$

We now investigate the effect of Marangoni flows resulting from cooling the bottom substrate ($M < 0$), which would in
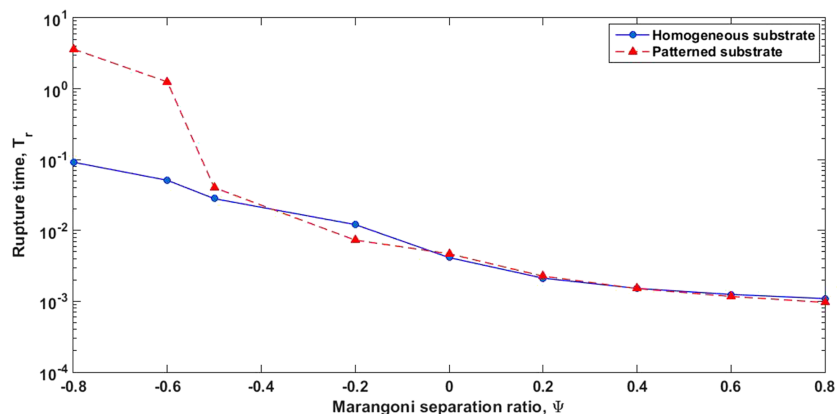

FIG. 14. The rupture time vs separation ratio Ψ when $M = 10$ for a homogeneous surface vs a chemically patterned surface having $w = 1.5\lambda$. Other parameters are the same as in Figs. 9–11.
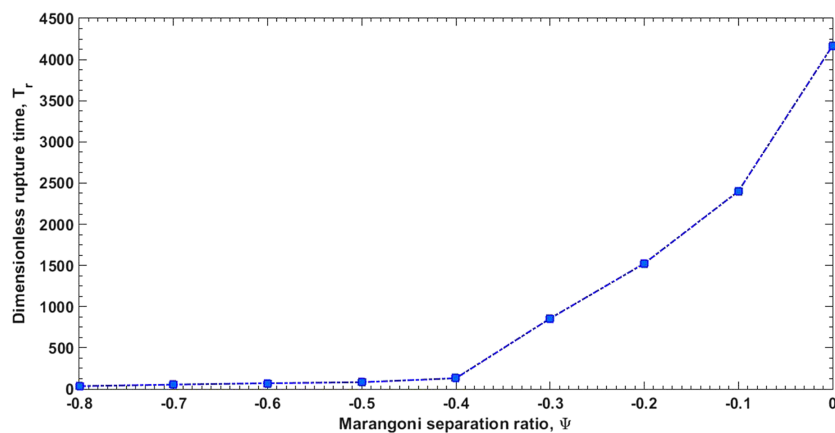
FIG. 15. Rupture time as a function of Ψ for a chemically patterned bottom surface when $M = -0.5$, $A = -10^{-3}$, $C^{-1} = 10^{-5}$, $B = 0.01$, $Sc = 100$, and $w = 0.5$ units.
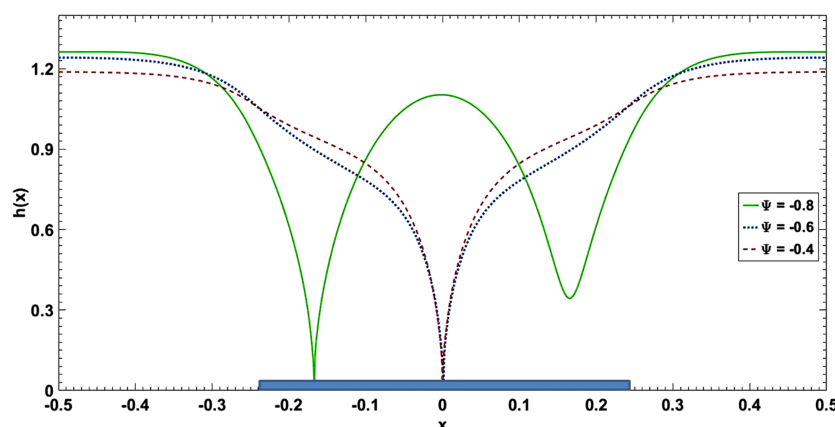

FIG. 16. Film height profiles at rupture when the bottom surface is chemically patterned, for parameters $M = -0.5$ and $w = 0.5$ units for three different values of the separation ratio Ψ: -0.8, -0.6, and -0.4. Other parameters are the same as in Fig. 15.

general oppose the van der Waals instability. With M set equal to -0.5, we tune the parameter Ψ in the negative as well as positive range. Figure 15 shows the rupture time variation as a function of Ψ on a chemically patterned bottom surface, with other parameters being $A = -10^{-3}$, $C^{-1} = 10^{-5}$, $B = 0.01$, and $Sc = 100$. Recall that the linear stability analysis (Fig. 3) predicts the film to be stable for $\Psi \geq 0$ in this parameter space for chemically homogeneous surfaces, while for $\Psi = -0.8$, there
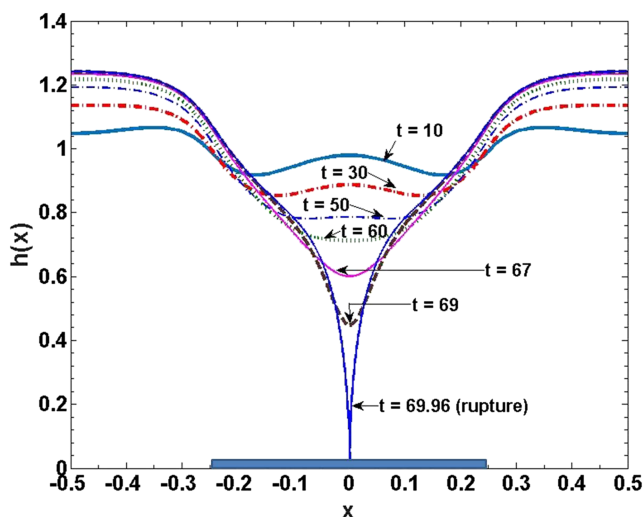

FIG. 17. Temporal evolution sequence of the film when $\Psi = -0.6$ for the parameters of interest in Fig. 16. The shaded region represents the less wettable patch of the chemically patterned surface.

would be an instability. A characteristic instability length λ cannot be identified for all values of Ψ. For uniformity, we use a domain length of 1 dimensionless unit, and a pattern width $w = 0.5$ at the center in all cases. In accordance with the linear theory, Fig. 15 suggests delays in the rupture time with Ψ becoming increasingly positive, especially steeply for $\Psi > -0.4$. However, the instability does kick in at very large times when $\Psi = 0$, due to wettability gradient driven flows. The different flow contributions for this case are as in Figs. 8(c) and 8(d) for $\Psi > 0$ and $\Psi < 0$, respectively. When $\Psi > 0$, the solutal flows ally with thermal Marangoni flows to flatten the surface and stabilize the film. But for $\Psi < 0$, a sufficiently strong contribution from thermodiffusion can assist the van der Waals forces which are in conflict with the Marangoni flows. The film is found to be remarkably stable for positive values of Ψ.

The rupture location for three different negative values of Ψ presents an interesting contrast, as seen in the film rupture profiles in Fig. 16. For $\Psi = -0.8$, one off-center rupture and another off-center near-rupture events are seen. This would have been originally expected, as the pattern width $w = 0.5$ is neither much smaller than the domain length to cause a centered rupture nor large enough to cause two independent ruptures at the boundaries of the patch. However, for $\Psi = -0.6$ and $\Psi = -0.4$, there is only one rupture, nearly centered. The mechanism of rupture may be understood through the temporal evolution sequence depicted in Fig. 17, for the representative case of $\Psi = -0.6$. The locations where depressions have formed at $t = 10$ are near the boundaries of the pattern,

initiated by the wettability gradients. These would also be the expected rupture locations, as seen in the rupture profile for $\Psi = -0.8$ [Fig. 16(a)]. But for $\Psi = -0.6$ and $\Psi = -0.4$, the thermodiffusion contribution that conflicts the thermal Marangoni flow is weaker [Fig. 8(d)]. It is now easier for the Marangoni flows to flatten the depressions that are observed at $t = 10$, by pushing liquid upwards to warmer regions. At $t = 50$, the free surface is nearly flat at the center and sloping upwards as we move sideways. With some thinning already present, the rupture is finally accomplished as a van der Waals instability, nearly symmetric about the center. The wettability gradients are inconsequential beyond a point in determining the rupture location. No evidence of oscillatory instability is seen, unlike in a similar situation for $M = 10$ seen in Sec. V D (Fig. 12).

VI. CONCLUSIONS

The current work extends the study of dynamics of non-isothermic thin liquid films of a binary miscible mixture by Bestehorn and Borcia[25] and Borcia et al.[56] In particular, the role of long-range intermolecular interactions like van der Waals forces and film behavior on wettability-patterned surfaces is examined, ignoring gravitational effects. These forces become important in ultrathin liquid films as thin as hundreds of nanometers. The linear stability analysis predicts that the oscillatory instability branch exists for positive values of M (heating from below), while for $M < 0$, the instability is monotonic. With attractive van der Waals forces, the film can be rendered stable only by adequately cooling the substrate from below. Increasingly positive values of the separation ratio Ψ assist the thermal contribution in accelerating the growth rate, when $M > 0$. If repulsive intermolecular forces are present, the critical Marangoni numbers to result in an instability are positive for all separation ratios from -1 to 1.

If the bottom surface on which the film rests is chemically patterned by wettability gradients, the dynamics is more complex. Rupture times and profiles can be profoundly modulated for patterns of different sizes by varying the strength and relative direction of the Soret effect. Within certain parameter spaces, the presence of wettability gradients could result in an oscillatory instability. This could also possibly delay ruptures significantly in comparison to the film rupture on chemically homogeneous surfaces. By using suitable combinations of heating/cooling, the choice of fluids with different sense of migration by thermodiffusion, and their relative strengths, a variety of different rupture behaviors can be obtained. This would help in the creation of various liquid morphologies which is useful in applications that rely on templating. Besides, the results on instability examined here would be important in microfluidics-based applications which employ temperature gradients to move around liquids confined to a certain area.[63]

A more focused set of simulations can target the development of pattern regime maps or phase diagrams that predict the nature of instability (oscillatory or monotonic) and the rupture location on a 3-D space of Ψ, M, and the pattern width. A short range Born repulsion would further help in capturing the

transition of a film to steady states like isolated droplet formation or coarsening, especially through 3D simulations. With transitions across steady states, a weakly nonlinear analysis might as well be able to provide new analytical insights into the nonlinear effects. These aspects may be probed as more challenging future extensions of the present work. Yet another practically useful strategy would be localized heating and/or cooling of the less (or more) wettable areas of a pattern. In that case, the length scale of the heated and cooled areas is also important in addition to the pattern dimensions.[60] Such selective heating and cooling of micron-sized patterns are achievable in practice through programmable microheaters and adaptive cooling devices.[64,65]

APPENDIX: COEFFICIENTS OF THE GROWTH RATE EXPRESSION

The coefficients of the dispersion relation (11) in Sec. III are as follows:

$$a_1 = -A + \frac{BM(2 + \Psi/2 - B\Psi/2)}{2(1+B)^2}, \tag{A1}$$

$$a_2 = -\frac{M\Psi}{2}, \tag{A2}$$

$$a_3 = \frac{\gamma_0}{3}, \tag{A3}$$

$$b_1 = \frac{5AB}{8(1+B)} - \frac{B(2+B)}{2S(1+B)} - \frac{MB^2(1 - B\Psi/2)}{3(1+B)^3}, \tag{A4}$$

$$b_2 = \frac{MB\Psi}{3(1+B)} - \frac{1}{S}, \tag{A5}$$

$$b_3 = \frac{-5B\gamma_0}{24(1+B)}. \tag{A6}$$

[1] R. Mukherjee and A. Sharma, "Instability, self-organization and pattern formation in thin soft films," Soft Matter **11**, 8717–8740 (2015).

[2] G. Amarandei, P. Beltrame, I. Clancy et al., "Pattern formation induced by an electric field in a polymer-air-polymer thin film system," Soft Matter **8**, 6333–6349 (2012).

[3] M. Ramanathan and S. B. Darling, "Mesoscale morphologies in polymer thin films," Prog. Polym. Sci. **36**, 793–812 (2011).

[4] N. Bhandaru, A. Das, and R. Mukherjee, "Confinement induced ordering in dewetting of ultra-thin polymer bilayers on nanopatterned substrates," Nanoscale **8**, 1073–1087 (2016).

[5] C. K. Sarika, G. Tomar, and J. K. Basu, "Pattern formation in thin films of polymer solutions: Theory and simulations," J. Chem. Phys. **144**(2), 024902 (2016).

[6] R. Konnur, K. Kargupta, and A. Sharma, "Instability and morphology of thin liquid films on chemically heterogeneous substrates," Phys. Rev. Lett. **84**, 931–934 (2000).

[7] K. Kargupta, R. Konnur, and A. Sharma, "Instability and pattern formation in thin liquid films on chemically heterogeneous substrates," Langmuir **16**(26), 10243–10253 (2000).

[8] D. Simmons and A. Chauhan, "Influence of physical and chemical heterogeneity shape on thin film rupture," J. Colloid Interface Sci. **295**, 472–481 (2006).

[9] R. D. Lenz and S. Kumar, "Competitive displacement of thin liquid films on chemically patterned substrates," J. Fluid Mech. **571**, 33–57 (2007).

[10] V. S. Ajaev, E. Y. Gatapova, and O. A. Kabov, "Rupture of thin liquid films on structured surfaces," Phys. Rev. E **84**, 041606 (2011).

[11] A. Patra, D. Bandyopadhyay, G. Tomar, A. Sharma, and G. Biswas, "Instability and dewetting of ultrathin solid viscoelastic films on homogeneous and heterogeneous substrates," J. Chem. Phys. **134**(6), 064705 (2011).

[12] K. Kargupta and A. Sharma, "Dewetting of thin films on periodic physically and chemically patterned surfaces," Langmuir **18**(5), 1893–1903 (2002).

[13] K. Kargupta and A. Sharma, "Morphological self-organization by dewetting in thin films on chemically patterned substrates," J. Chem. Phys. **116**(7), 3042–3051 (2002).

[14] K. Kargupta and A. Sharma, "Mesopatterning of thin films by templating on chemically patterned complex substrates," Langmuir **19**(12), 5153–5163 (2003).

[15] J. C.-T. Kao, A. A. Golovin, and S. H. Davis, "Rupture of thin films with resonant substrate patterning," J. Colloid Interface Sci. **303**, 532–545 (2006).

[16] X. He, F. Gao, G. Tu *et al.*, "Formation of nanopatterned polymer blends in photovoltaic devices," Nano Lett. **10**, 1302–1307 (2010).

[17] K. Yim, W. Doherty, W. Salaneck, C. E. Murphy, R. H. Friend, and J. Kim, "Phase-separated thin film structures for efficient polymer blend light-emitting diodes," Nano Lett. **10**, 385–392 (2010).

[18] L. Xue and Y. Han, "Pattern formation by dewetting of polymer thin film," Prog. Polym. Sci. **36**(2), 269–293 (2011).

[19] T. M. Squires and S. R. Quake, "Microfluidics: Fluid physics at the nanoliter scale," Rev. Mod. Phys. **77**(3), 977–1026 (2005).

[20] S. J. Lee and S. Y. Lee, "Micro total analysis system in biotechnology," Appl. Microbiol. Biotechnol. **64**(3), 289–299 (2004).

[21] S. H. Davis, "Thermocapillary instabilities," Annu. Rev. Fluid Mech. **19**, 403–435 (1987).

[22] F. Takabatake, K. Yoshikawa, and M. Ichikawa, "Mode bifurcation of droplet motion under stationary laser irradiation," J. Chem. Phys. **141**(5), 051103 (2014).

[23] J. K. Platten, "The Soret effect: A review of recent experimental results," J. Appl. Mech. **73**, 5–15 (2006).

[24] D. T. J. Hurle and E. Jakeman, "Soret driven thermosolutal convection," J. Fluid Mech. **47**, 667–687 (1971).

[25] M. Bestehorn and I. D. Borcia, "Thin film lubrication dynamics of a binary mixture: Example of an oscillatory instability," Phys. Fluids **22**, 104102 (2010).

[26] A. Oron, S. H. Davis, and S. G. Bankoff, "Long-scale evolution of thin liquid films," Rev. Mod. Phys. **69**(3), 931–980 (1997).

[27] R. V. Craster and O. K. Matar, "Dynamics and stability of thin liquid films," Rev. Mod. Phys. **81**, 1131–1198 (2009).

[28] S. K. Kalpathy, L. F. Francis, and S. Kumar, "Shear-induced suppression of rupture in two-layer thin liquid films," J. Colloid Interface Sci. **348**, 271–279 (2010).

[29] S. K. Kalpathy, L. F. Francis, and S. Kumar, "Thin-film models of liquid displacement on chemically patterned surfaces for lithographic printing processes," J. Colloid Interface Sci. **383**, 155–166 (2012).

[30] M. Dietzel and S. M. Troian, "Formation of nanopillar arrays in ultrathin viscous films: The critical role of thermocapillary stresses," Phys. Rev. Lett. **103**, 074501 (2009).

[31] M. Dietzel and S. M. Troian, "Thermocapillary patterning of nanoscale polymer films," in *Three Dimensional Micro- and Nanoscale Fabrication and Lithography*, edited by S. M. Kuebler and V. T. Milam (Materials Research Society, 2009), p. 1179–BB08–02.

[32] E. McLeod, Y. Liu, and S. M. Troian, "Experimental verification of the formation mechanism for pillar arrays in nanofilms subject to large thermal gradients," Phys. Rev. Lett. **106**, 175501 (2011).

[33] O. Lyutakov, J. Tuma, I. Huttel, V. Prajzler, J. Siegel, and V. Svorcik, "Polymer surface patterning by laser scanning," Appl. Phys. B **110**(4), 539–549 (2013).

[34] J. Trice, C. Favazza, D. Thomas, H. Garcia, R. Kalyanaraman, and R. Sureshkumar, "Novel self-organization mechanism in ultrathin liquid films: Theory and experiment," Phys. Rev. Lett. **101**, 017802 (2008).

[35] J. P. Burelbach, S. G. Bankoff, and S. H. Davis, "Nonlinear stability of evaporating/condensing liquid films," J. Fluid Mech. **195**, 463–494 (1988).

[36] A. Pototsky, M. Bestehorn, and D. Merkt, "Morphology changes in the evolution of liquid two-layer films," J. Chem. Phys. **122**, 224711 (2005).

[37] A. A. Nepomnyashchy and I. B. Simanovskii, "Decomposition of a two-layer thin liquid film flowing under the action of Marangoni stresses," Phys. Fluids **18**, 112101 (2006).

[38] A. A. Nepomnyashchy and I. B. Simanovskii, "Marangoni instability in ultrathin two-layer films," Phys. Fluids **19**, 122103 (2007).

[39] A. Zebib, "Stability of ternary and binary mixtures in a vertical slot including the Soret effect," J. Chem. Phys. **129**(13), 134711 (2008).

[40] K. C. Sahu, H. Ding, P. Valluri, and O. K. Matar, "Linear stability analysis and numerical simulation of miscible two-layer channel flow," Phys. Fluids **21**, 042104 (2009).

[41] A. Sharma and J. Mittal, "Instability of thin liquid films by density variations: A new mechanism that mimics spinodal dewetting," Phys. Rev. Lett. **89**, 186101 (2002).

[42] L. Talon and E. Meiburg, "Plane Poiseulle flow of miscible layers with different viscosities: Instabilities in the Stokes flow regime," J. Fluid Mech. **686**, 484–506 (2011).

[43] H. Ding, P. D. M. Spelt, and C. Shu, "Diffuse interface model for incompressible two-phase flows with large density ratios," J. Comput. Phys. **226**, 2078–2095 (2007).

[44] S. Madruga and U. Thiele, "Decomposition driven interface evolution for layers of binary mixtures: II. Influence of convective transport on linear stability," Phys. Fluids **21**, 062104 (2009).

[45] L. O. Naraigh and J. Thiffeault, "Nonlinear dynamics of phase separation in thin films," Nonlinearity **23**, 1559–1583 (2010).

[46] N. Clarke, "Instabilities in thin-film binary mixtures," Eur. Phys. J. E **14**, 207–210 (2004).

[47] S. Shklyaev, A. A. Nepomnyashchy, and A. Oron, "Oscillatory long-wave Marangoni convection in a binary liquid: Rhombic patterns," SIAM J. Appl. Math. **73**(6), 2203–2223 (2013).

[48] S. Shklyaev, A. A. Nepomnyashchy, and A. Oron, "Three-dimensional oscillatory long-wave Marangoni convection in a binary liquid layer with the Soret effect: Bifurcation analysis," Phys. Fluids **19**(7), 072105 (2007).

[49] S. Shklyaev, A. A. Nepomnyashchy, and A. Oron, "Marangoni convection in a binary liquid layer with Soret effect at small Lewis number: Linear stability analysis," Phys. Fluids **21**(5), 054101 (2009).

[50] M. Morozov, A. Oron, and A. A. Nepomnyashchy, "Nonlinear dynamics of long-wave Marangoni convection in a binary mixture with the Soret effect," Phys. Fluids **25**(5), 052107 (2013).

[51] S. Shklyaev, A. A. Nepomnyashchy, and A. Oron, "Longwave oscillatory convection in a binary liquid: Hexagonal patterns," Europhys. Lett. **86**, 14005 (2009).

[52] I. S. Fayzrakhmanova, S. Shklyaev, and A. A. Nepomnyashchy, "Longwave convection in a layer of binary mixture with modulated heat flux: Weakly nonlinear analysis," Fluid Dyn. Res. **46**, 041411 (2014).

[53] A. Podolny, A. Oron, and A. A. Nepomnyashchy, "Linear and nonlinear theory of long-wave Marangoni instability with the Soret effect at finite Biot numbers," Phys. Fluids **18**(5), 054104 (2006).

[54] A. Podolny, A. A. Nepomnyashchy, and A. Oron, "Long-wave Marangoni instability in a binary liquid layer on a thick solid substrate," Phys. Rev. E **76**(2), 026309 (2007).

[55] A. Podolny, A. Oron, and A. A. Nepomnyashchy, "Long-wave Marangoni instability in a binary liquid layer with deformable interface in the presence of Soret effect: Linear theory," Phys. Fluids **17**(10), 104104 (2005).

[56] R. Borcia, I. D. Borcia, and M. Bestehorn, "Nonlinear dynamics of thin liquid films consisting of two miscible components," Phys. Rev. E **86**, 056319 (2012).

[57] J. L. Castillo and M. G. Velarde, "Thermal diffusion and the Marangoni Benard instability of a two-component fluid layer heated from below," Phys. Lett. A **66**, 489–491 (1978).

[58] M. Bestehorn and P. Colinet, "Benard Marangoni convection of a binary mixture as an example of an oscillatory bifurcation under strong symmetry-breaking effects," Physica D **145**, 84–109 (2000).

[59] H. C. Hamaker, "The London van der Waals attraction between spherical particles," Physica **4**, 1058–1072 (1937).

[60] S. K. Kalpathy, L. F. Francis, and S. Kumar, "Thermally induced delay and reversal of liquid film dewetting on chemically patterned surfaces," J. Colloid Interface Sci. **408**, 212–219 (2013).

[61] M. C. Cross and P. C. Hohenberg, "Pattern formation outside of equilibrium," Rev. Mod. Phys. **65**(3), 851–1124 (1993).

[62]N. Tiwari and J. M. Davis, "Stability of a volatile liquid film spreading along a heterogeneously-heated substrate," J. Colloid Interface Sci. **355**(1), 243–251 (2011).

[63]A. Gunther and K. F. Jensen, "Multiphase microfluidics: From flow characteristics to chemical and materials synthesis," Lab Chip **6**, 1487–1503 (2006).

[64]A. A. Darhuber, J. P. Valentino, S. M. Troian, and S. Wagner, "Thermocapillary actuation of droplets on chemically patterned surfaces by programmable microheater arrays," J. Microelectromech. Syst. **12**(56), 873–879 (2003).

[65]P. Y. Paik, V. K. Pamula, and K. Chakrabarty, "Adaptive cooling of integrated circuits using digital microfluidics," IEEE Trans. Very Large Scale Integr. Syst. **16**(4), 432–443 (2008).